Qualitative interpretation of electron energy-loss near-edge structure in natural zircon

1992 J. Phys.: Condens. Matter 4 8363

(http://iopscience.iop.org/0953-8984/4/43/011)

J. Phys.: Condens. Matter 4 (1992) 8363–8374. Printed in the UK

Qualitative interpretation of electron energy-loss near-edge structure in natural zircon

D W McComb†||, R Brydson‡, P L Hansen§ and R S Payne†

† Microstructural Physics Group, Cavendish Laboratory, Madingley Rd, Cambridge CB3 0HE, UK
‡ University of Oxford, Dept. of Materials, Parks Rd, Oxford OX1 3PH, UK
§ Laboratory of Applied Physics, Technical University of Denmark, 2800 Lyngby, Denmark

Received 30 April 1992

Abstract. The results of an electron energy-loss spectroscopy (EELS) study of zircon are reported. It is shown that the oxygen K-shell, and the silicon K- and $L_{2,3}$-shell excitations exhibit near-edge structure significantly different to that observed in other nesosilicates. The spectra have been modelled using multiple-scattering calculations, and these results, combined with results from molecular orbital calculations, have enabled assignment of most of the features in the energy-loss spectra to particular electronic transitions. It is concluded that ELNES 'fingerprints' are associated not with coordination, but with the symmetry at the central atom site.

1. Introduction

Electron energy-loss spectroscopy (EELS) carried out in the electron microscope is now a well established technique for the measurement of chemical composition with high spatial resolution [1]. The energy-loss near-edge structure (ELNES) of inner-shell ionization edges can also be used to gain insight into the chemical and structural properties of the atom undergoing excitation [2]. In this paper a study of the electron energy-loss excitations observed in natural zircon is reported.

Zircon is a common mineral with nominal composition, $ZrSiO_4$, often used as a source of zirconium oxide and zirconium metal. The mineral exhibits a tetragonal crystal system with space group $I4_1/amd$ (a = 6.607 Å, c = 5.982 Å) [3]. The structure of zircon, shown in figure 1, is based on chains, parallel to the c-axis, of alternating edge-sharing SiO_4 tetrahedra and ZrO_8 triangular dodecahedra. The chains are interconnected by edge-sharing dodecahedra. Zircon is classed as a nesosilicate because no two SiO_4 units are linked directly, but only through ZrO_8 polyhedra. It is worth noting that the zirconium atoms are in a direct line-of-sight from the silicon atoms.

|| From 1 July 1992 at: Steacie Institute of Molecular Sciences, National Research Council, Ottawa, Ontario, Canada.

0953-8984/92/438363+12$07.50

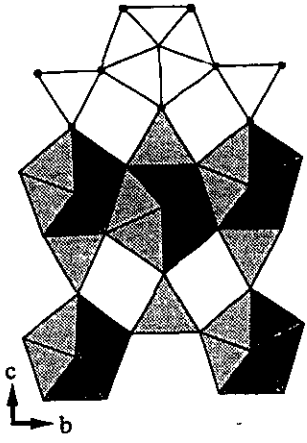

Figure 1. Schematic diagram of the structure of zircon, $ZrSiO_4$. Shown are the chains of alternating edge-sharing SiO_4 'tetrahedra' and ZrO_8 triangular dodecahedra parallel to *c*, connected in the *b*-direction by edge-sharing dodecahedra.

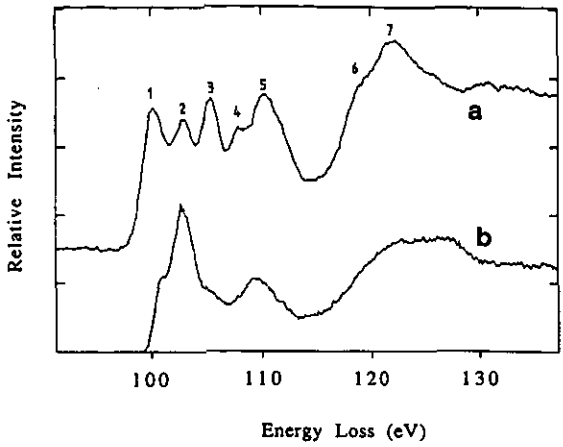

Figure 2. (*a*) Silicon $L_{2,3}$ edge of zircon, $ZrSiO_4$. For comparison the silicon $L_{2,3}$ edge of fayalite, Fe_2SiO_4, is shown; (*b*), this spectrum being typical of a material based on SiO_4 tetrahedra.

2. Methods and materials

The zircon sample, which originated from Ontario, Canada, was supplied by Microanalysis Consultants, UK (Set No 2373), in the form of small crystals dispersed on a holey carbon film, supported by a copper grid. The composition, as measured by x-ray microprobe analysis, was $Zr_{0.96}Si_{1.04}O_{4.00}$. It should be noted that, the cation environment aside, zircon is structurally similar to other nesosilicates, the spectra for which we have previously reported [4, 5].

EELS was carried out using two different microscope and acquisition systems, both of which were operated at an accelerating voltage of 100 kV. The silicon $L_{2,3}$ edges and silicon L_1 edges were collected on a VG HB501 dedicated scanning transmission electron microscope (STEM) using a recently developed parallel recording system [6]. All of these spectra were acquired in image mode using an effective collection angle of 8.3 mrad. The energy resolution measured by the full-width at half maximum (FWHM) of the zero-loss peak was 0.6 eV. The oxygen and silicon K-shell excitations were also collected using the system described above, but an effective collection angle of approximately 16 mrad was used. The zirconium $L_{2,3}$ edge was collected using a Phillips CM30 transmission electron microscope (TEM) fitted with an LaB_6 filament and a Gatan 666 parallel EELS system. The spectra were recorded in image coupled mode using an effective collection angle of 9.2 mrad with an energy resolution of 0.9 eV FWHM.

Zircon is relatively resistant to electron-beam damage, and no changes in the spectra due to total dose or dose-rate effects were observed in the time necessary to obtain good spectrum statistics. A background of the form, AE^{-r}, fitted to the pre-edge region, was removed from each core-loss edge. The spectra were not deconvoluted to remove contributions due to multiple energy losses; however, such multiple scattering does not have a large influence on the ELNES in the region of interest, i.e. 0–15 eV, above the threshold energy. No attempt was made to investigate

the effect of crystal orientation on the energy-loss spectrum.

3. Experimental results

The silicon $L_{2,3}$ edge is shown in figure 2. The spectrum is very different to that of silica [7], and also those of the nesosilicates previously reported [4], implying that the concept of a simple coordination fingerprint [2] for the SiO_4 tetrahedron is fundamentally flawed. In particular from 0–15 eV above the threshold energy five very sharp peaks are observed. The angular variance of the silicate tetrahedron in zircon is 97.8 (deg^2), as measured from the single-crystal XRD study [8], and based on previous work it would be predicted that the silicon $L_{2,3}$ edge in zircon should be very broad due to this large angular variance [4]. It is certainly true that the silicon $L_{2,3}$ edge in zircon exhibits more structure, over a wider energy range than is observed in, say, α-quartz or fayalite (Fe_2SiO_4), but without detailed theoretical calculations it is difficult to describe the origin of this fine structure.

The silicon L_1 and K edges should be essentially identical since the initial state in both cases is an s-type atomic orbital; the dipole selection rule forbids s $\rightarrow$ s transitions, so the ELNES at both edges should be a representation of the p-projected density of empty states at the silicon site. Any differences between the L_1- and K-shell edges could be attributed to (*a*) changes in the core-hole lifetime at the silicon 2s and 1s core levels, respectively, and (*b*) variations in the matrix elements for the $ns \rightarrow$ p transitions, where n is the principal quantum number. Experimentally the L_1 edge (not shown) is found to be almost identical to the K edge (figure 3(*a*)), indicating that at this energy resolution differences in these quantities have little effect on the observed ELNES.

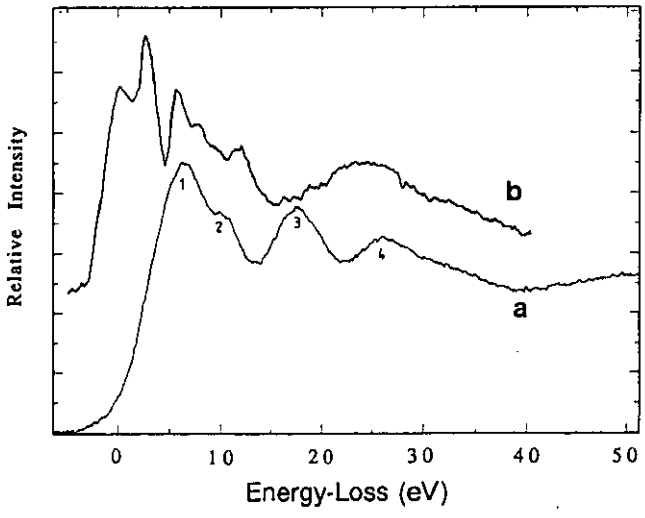

Figure 3. Plots showing the silicon K edge, (*a*), and the oxygen K edge, (*b*), in zircon.

The oxygen K edge is compared with the silicon K edge in figure 3, and immediately emphasizes the need to treat core-loss spectroscopy as a probe of the

local unoccupied energy levels, since in an extended band-structure model these edges should be very similar. More significantly, the silicon and oxygen K edges in zircon are considerably different to those found in other silicate minerals [5].

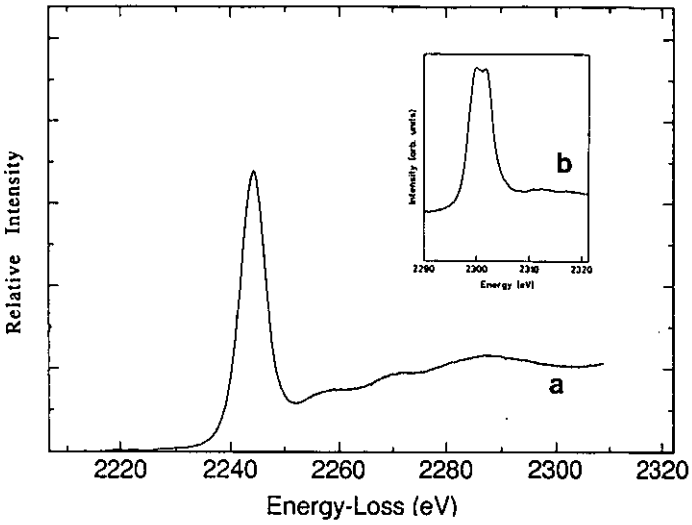

Figure 4. Plot of the zirconium L_3 edge in zircon. Inset: the x-ray absorption spectrum of the L_2 edge of zirconium in ZrO_2 [9].

The zirconium L_3 edge is shown in figure 4. (The L_2 edge was also recorded but is not displayed.) The spectrum shows a 'white line' feature typical of transition metal L edges. The zirconium $L_{2,3}$ edge of ZrO_2 was also measured, and was found to be identical to that of zirconium in zircon. However, x-ray absorption spectroscopy (XAS) has shown that in ZrO_2 the zirconium L_2 edge, and therefore the L_3 edge, is split into two peaks separated by 2.1–2.4 eV [9]. These two peaks arise due to crystal-field splitting of the zirconium 4d orbitals, but such a splitting is not apparent in the energy-loss spectrum of either zircon or ZrO_2. Crystal-field theory indicates that a splitting of the 4d orbitals should occur in both cases, and this should be observable at 0.9 eV resolution. It is concluded that the electrostatic offset of > 2 keV used to record the ELNES at the zirconium $L_{2,3}$ edge substantially degrades the energy resolution by defocusing the energy-loss spectrum. On the basis of the XAS spectrum of ZrO_2 it is suggested that a crystal-field splitting in the range 2.1–2.4 eV is present at the zirconium L_3 edge in zircon, and further work to confirm this using EELS is at present under way.

The main objective is to obtain a complete description of the observed ELNES for zircon. An attempt is made to achieve this through combined knowledge of EELS, molecular orbital (MO) theory and the theory of x-ray absorption near-edge structure (XANES).

4. Theoretical approaches to ELNES

As a starting point to understanding the energy-loss spectra of zircon it is useful to consider the various molecular orbitals available as final states into which core

electrons can be excited. The results of an SCF–X_α MO calculation for the SiO_4^{4+} tetrahedron have been reported by Tossel [10]. In a study of EELS of nesosilicates, it was shown that from this calculation a reasonable interpretation of the silicon $L_{2,3}$ edges could be obtained [4]. However, to achieve this it was necessary to reverse the ordering of the first two unoccupied MOs, i.e. $6t_2 + 6a_1$. This reversal is consistent not only with experimental results of other workers [18, 19], but also with band-structure calculations on α-quartz which predict that the lowest conduction band is predominantly s-like [20]. The MO diagram obtained by Tossel is reproduced in figure 5(*a*), but the above comments should be remembered when comparing this diagram with the experimental results.

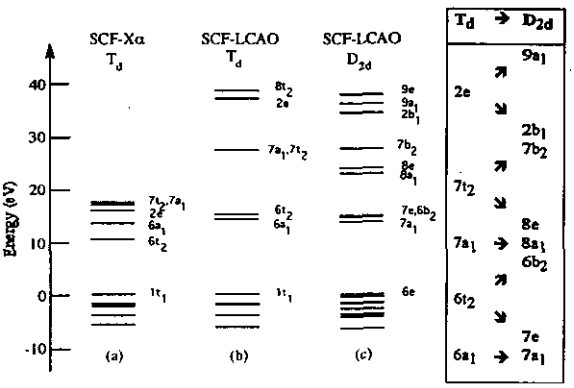

Figure 5. Molecular orbital diagrams for an SiO_4^{4-} polyhedron with T_d symmetry calculated using the, (*a*) SCF–X_α, and, (*b*) SCF-LCAO methods. The results of an SCF-LCAO calculation for SiO_4^{4-} with D_{2d} symmetry are shown in (*c*). The schematic diagram illustrates the splitting of the MOs which occurs on lowering the symmetry from T_d to D_{2d}.

As mentioned earlier the SiO_4 polyhedron in zircon is considerably distorted, indicated by the high angular variance, presumably due to the strong influence of the ZrO_8 dodecahedra. As a result the symmetry of the silicate unit is lowered from approximately tetrahedral, T_d, as found in α-quartz etc., to D_{2d}, where the major rotation axis is twofold rather than threefold as in the undistorted case. MO calculations for SiO_4^{4-} in both T_d and D_{2d} symmetry have been carried out using the GAUSSIAN 90 SCF-LCAO code of Frisch *et al* [11]. In both cases a 6-31G* basis set was used [22]. The results are shown in figure 5. The main point of interest is the way in which, on lowering the symmetry of the polyhedron from T_d to D_{2d}, degenerate MOs in the undistorted tetrahedron are split into two distinct MOs as illustrated by the schematic diagram in figure 5.

Figure 5 clearly shows that there are significant differences between the SCF-LCAO and the SCF–X_α results for the T_d SiO_4^{4-} cluster. In particular, the position of the d-like MO, 2e, is sensitive to the method of calculation, and it is not immediately obvious why this should be so. Previously published results of SCF-LCAO calculations on isoelectronic clusters show ordering of the unoccupied MOs which is identical to that shown in figure 5(*b*) [21]. However, as will be shown later, multiple-scattering theory produces results that are more consistent with the MO levels predicted by the

X_α method. At present no judgement is made as to which calculation method is correct. It is assumed that an SCF-X_α MO diagram for an SiO_4 cluster with D_{2d} symmetry would show splitting of the degenerate MOs in a similar manner to that found using the SCF-LCAO method. On this basis, interpretations of the observed ELNES using both the SCF-Xα and SCF-LCAO theoretical results will be proposed.

Multiple-scattering (MS) theory is based on the interference between the outgoing electron wave of the ejected electron and the electron wave which has been backscattered from the surrounding atoms [2]. MS theory was originally developed for the study of x-ray absorption near-edge structure (XANES), the x-ray equivalent of ELNES, and for this reason the computations are often called XANES calculations. The calculations are performed in real space using a cluster approach; the atomic species of interest is placed in the centre of the cluster, surrounded by the atoms forming the first coordination shell. Higher-order coordination shells can also be included, and, while there is evidence that the gross features in ELNES may be reproduced using only the nearest-neighbour shell [2], it has been shown that, in some cases, a very close fit to the energy-loss spectrum may be achieved by using a large number of shells [12].

The calculations were carried out using the ICXANES program of Vvedensky *et al* [13]. Initially phase shifts and matrix elements for the MS calculations were obtained by imposing a muffin-tin form of the potential on the crystal structure of $ZrSiO_4$. However, since zircon is a relatively open structure this muffin-tin form of the potential is a poor approximation to the actual potential in this crystal. It is also very difficult to minimize the discontinuities in potential at the touching muffin-tin spheres. Consequently, to circumvent this problem, phase shifts for oxygen and silicon were obtained from a muffin-tin potential calculation on the more close-packed structure of α-SiO_2—which appears to give reliable results. The relevant phase shifts for zirconium were obtained from the muffin-tin calculation on zircon, and then adjusted in energy so that they corresponded to the same muffin-tin zero of energy as in the α-SiO_2 calculation. Although this procedure is far from satisfactory, it is necessary to possess reliable scattering phase shifts for oxygen since most of the scattering will be determined by the oxygen atoms. Nevertheless, the phase shifts for zirconium are likely to be a poor representation of the true scattering properties; this is discussed below with reference to the MS calculation of the oxygen K-shell edge. The influence of the core hole present in the excited state is accounted for through the $Z + 1^*$ approximation [2], which estimates that the effect of the core hole is to increase the nuclear charge perceived by the outer electrons by one unit.

5. Zircon—a theoretical interpretation

5.1. Silicon K edge

The silicon K ELNES in zircon arises from transitions from the silicon 1s core level to empty states with p-like symmetry projected from the silicon atom. It shows four main features, labelled 1–4 in figure 3(*a*). Comparison with the silicon K edge in α–quartz [6], which exhibits only two main features in the near-edge region, indicates that this is considerably more complex than the standard silicon K edge for an SiO_4 unit. This complexity is attributed to the large distortion present in $ZrSiO_4$, which, as discussed above, lowers the symmetry at the silicon site from T_d to D_{2d}.

From MO theory, the allowed dipole transitions in T_d symmetry are from the silicon 1s core level to the MOs labelled t_2 in figure 5. Hence, in relatively undistorted

silicates such as α-quartz and fayalite, two peaks are expected at the silicon K edge corresponding to transitions to the two t_2 MOs. This has been confirmed by experiment [5]. On going from T_d to D_{2d} symmetry, the SCF-LCAO MO calculations (figure 5(*c*)) indicate that each of the t_2 MOs splits into two distinct levels, e and b_2. Under the dipole selection rule, transitions to both of these levels are allowed [14]. Therefore, four separate features are observed at the silicon K edge of zircon. This splitting of the two t_2 MOs would also occur in the SCF-X_α method, and therefore both MO calculation methods predict the same result.

The results of MS calculations on clusters consisting of a single shell support the MO interpretation. For a perfect SiO_4 tetrahedron a single strong peak at the edge onset followed by a less intense shoulder at higher energy loss is observed (figure 6). On increasing the number of shells this basic structure remains unchanged, except that the intensity of the shoulder increases relative to the first strong peak. This agrees with experimental observations for α-quartz in which the SiO_4 tetrahedron is only slightly distorted. For a D_{2d} SiO_4 polyhedron as found in zircon, the first strong peak is seen to split into two features (figure 6(*b*)). On increasing the size of this cluster this splitting is enhanced, and furthermore, a splitting of the high-energy shoulder is observed. The resulting MS calculation (figure 6(*c*)) for the silicon K ELNES of a seven-shell zircon cluster reproduces all four features in terms of relative energy positions; however, the relative intensities are somewhat in error due to the difficulties outlined earlier.

The influence of the zirconium atoms in the cluster was investigated by performing MS calculations on a zircon-like cluster minus the zirconium atoms. The general effect of the zirconium atoms on the silicon K edge was to add intensity into peaks 3 and 4 in the calculated spectrum.

It is concluded that, although the splitting of the initial peak (peaks 1 and 2) may be reproduced using a single-shell calculation, the p-like DOS is in reality considerably delocalized, and is sensitive to the effects of longer-range distortions which result in the splitting of peaks 3 and 4. Hence it is only meaningful to describe peaks 1 and 2 in the experimental spectrum in terms of transitions to the specific MOs, 7e and $6b_2$.

5.2. Silicon $L_{2,3}$ edge

The silicon $L_{2,3}$ edge in zircon is very different to that found in other nesosilicates, such as fayalite. In fayalite, Fe_2SiO_4, the silicon $L_{2,3}$ edge exhibits four main features that have been previously assigned to transitions from the silicon 2p core level to the $6a_1$ (s-like), $6t_2$ (p-like), 2e (d-like), and $7t_2$ (d-like) MOs of an SiO_4 cluster of T_d symmetry (figure 5(*a*)) [4]. As discussed in an earlier publication [15], transitions from the silicon 2p level to the t_2 (p-like) MO are in fact dipole allowed owing to the lack of inversion symmetry at the silicon site which results in significant p–d mixing. The above assignment was carried out using the SCF-Xα result in figure 5(*a*) [10]. Using the SCF-LCAO results (figure 5(*b*)) the first two peaks would have the same assignment as above, i.e. $6a_1 + 6t_2$, but peak 3 would be assigned to the closely spaced MOs labelled $7a_1$, $7t_2$ in figure 5(*b*), while peak 4 would be associated with the higher energy MO, 2e.

Comparing the silicon $L_{2,3}$ ELNES of fayalite and zircon (figure 2), it is possible to derive a qualitative explanation for the presence of seven peaks at the silicon $L_{2,3}$ edge of zircon in terms of the lowering of symmetry from T_d to D_{2d}. It is clearly shown in figure 5 that on going from T_d and D_{2d} symmetry splitting of the t_2 and e MOs occurs. As mentioned above, the t_2 level splits into MOs of e and b_2 symmetry,

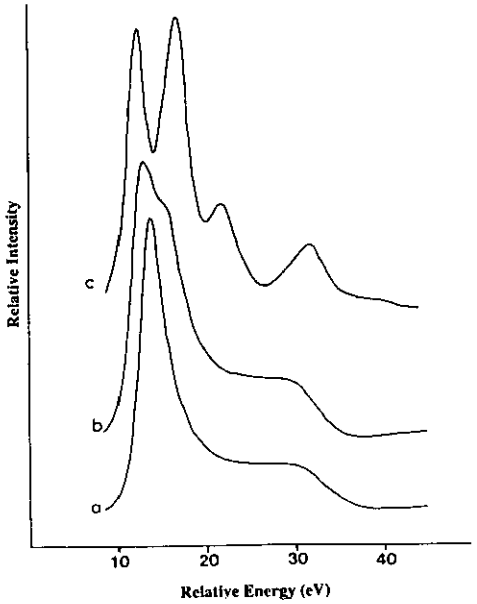

Figure 6. Plots showing the results of the MS calculations for the silicon K ELNES. Shown are the results of calculations for single-shell clusters with, (*a*) T_d symmetry, and, (*b*) D_{2d} symmetry. A calculation for a seven-shell cluster with D_{2d} symmetry, (*c*), is also shown.

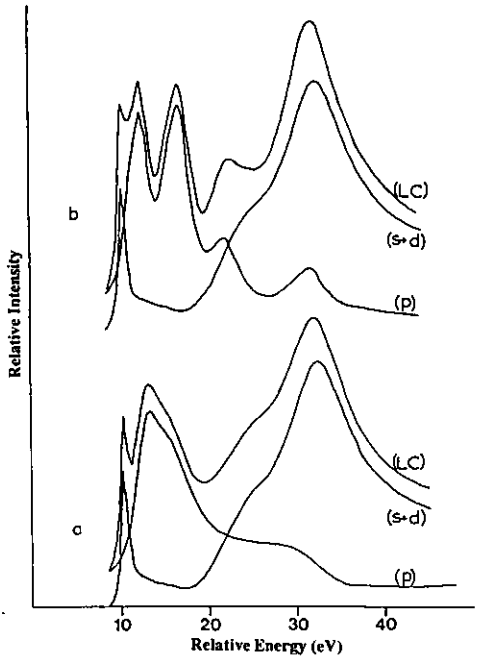

Figure 7. Plots showing the results of MS calculations for the silicon $L_{2,3}$ edge in zircon. Shown are the results of calculations of the s+d and p contributions for clusters consisting of one coordination shell, (*a*), and seven coordination shells, (*b*). A linear combination (LC) of the s+d and p contributions is also shown for comparison with the experimental data.

while the e MO is split into b_1 and a_1 levels. On this basis all seven features in the silicon $L_{2,3}$ edge of zircon may be assigned to specific molecular orbitals (table 1).

Table 1. MO assignments for the peaks at the silicon $L_{2,3}$ edge for SiO_4 polyhedra with T_d symmetry (e.g. fayalite) and D_{2d} symmetry (e.g. zircon). Shown are the assignments based on both the SCF–X_α and SCF-LCAO methods for calculation of MOs.

SiO_4T_d (e.g. fayalite—figure 2(*a*))			SiO_4D_{2d} (e.g. zircon—figure 2(*b*))		
	MO assignment			MO assignment	
Peak number	SCF–X_α	SCF-LCAO	Peak number	SCF–X_α	SCF-LCAO
1	$6a_1$	$6a_1$	1	$7a_1$	$7a_1$
2	$6t_2$	$6t_2$	2	7e	7e, $6b_2$
3	2e	$7a_1$, $7t_2$	3	$6b_2$	$8a_1$
4	$7t_2$	2e	4	$2b_1$	8e
			5	$9a_1$	$7b_2$
			6	8e	$2b_1$
			7	$7b_2$	$9a_1$

However, as mentioned above, this MO description appears only to be valid in the

first 10 eV or so above the threshold energy. Hence for a fuller picture of the silicon $L_{2,3}$ ELNES the results of MS calculations are necessary.

It has been shown previously that in order to model the silicon $L_{2,3}$ edge in silicates using MS theory (or in general, the $L_{2,3}$ edge of any tetrahedrally coordinated atom/ion) it is necessary to consider transitions to both d-like and s-like final states ($\Delta l = \pm 1$) as well as transitions to p-like final states [15]. This arises due to the spherically symmetric form of the muffin-tin approximation for the crystal potential which is needed to calculate the scattering phase shifts and atomic matrix elements for the MS calculation. This spherical symmetry does not implicitly include p–d mixing, and therefore transitions to p-like final states have to be artificially included to match experiment. For comparison with experimental results a linear combination of the (s+d) and p calculations was taken. No emphasis is placed on the coefficients used in the linear combination.

An MS calculation for a single shell cluster, i.e. SiO_4 in D_{2d} symmetry as in zircon (figure 7(*a*)), reproduces peak 1 which arises from s-like final states, and peaks 2 and 3 which mainly arise from the e–b_2 splitting of the p-like final states (although close inspection reveals that there is a similar splitting of the d-like final states which supports the argument for p–d mixing of final-state wavefunctions in non-centrosymmetric environments). Increasing the size of the cluster (figure 7(*b*)) indicates that although s- and d-like final states are essentially localized within the first coordination shell, the p-like DOS is modified by outer shells as was observed in the calculations of the silicon K ELNES. The overall result is to produce two further peaks in the p-like component (analogous to peaks 3 and 4 at the silicon K edge) which cause the splitting of peaks 4/5 and 6/7. Hence, peaks 4 and 6 at the silicon $L_{2,3}$ edge of zircon can be associated with p-like final states. As at the silicon K edge, the general effect of zirconium atoms is to contribute intensity to the third and fourth peaks of the p-like DOS.

The interpretation based on the MS calculations is in good agreement with that from the SCF–X_α MO results. This might be taken to indicate that the SCF–X_α method is more accurate than the SCF–LCAO approach. However, it should be remembered that the SCF–X_α and MS methods are essentially identical since they are both based on scattered-wave calculations. Therefore it would have been very surprising if they had failed to agree. The main point of note is that all of the theoretical methods predict the silicon $L_{2,3}$ edge of zircon to consist of substantially more peaks than found for α-quartz or fayalite. This occurs due to reduced symmetry at the silicon site in zircon, which results in removal of orbital degeneracies.

5.3. Oxygen K edge

The oxygen K edge of zircon also shows a very complex structure. However, broadly the shape follows that of the silicon K edge. This is to be expected since both excitations are probing the p-like DOS. However, the local nature of the excitation means that differences in the projections of the empty states at each site must also be considered. One major difference is that at the oxygen site the oxygen 2p orbitals can interact significantly with the zirconium 4d orbitals, as well as with the silicon 3s/3p and 3d orbitals. To a first approximation, the effect of the neighbouring zirconium atoms would be to split the p-like DOS accessible at the oxygen site by the crystal-field splitting of the 4d orbitals of Zr in zircon. This would occur through O 2p–Zr 4d hybridization. As mentioned earlier, XAS measurements indicate that this crystal-field splitting is between 2.1 and 2.4 eV [9]. While this is a useful starting point,

a recent MO calculation for a ZrO_8^{12-} polyhedron with D_{2d} symmetry, as found in zircon, exhibits a complex crystal-field splitting consisting of four distinct levels for the unoccupied 4d orbitals [16].

Examination of the oxygen K ELNES of zircon (figure 3(*b*)) suggests that the structure may be divided into two distinct regions. The first of these, from the energy threshold to about 6 eV above the onset, is associated with transitions to zirconium 4d dominated empty states which are hybridized with oxygen 2p orbitals. As mentioned above, the zirconium 4d orbitals will be split into t_{2g}-like and e_g-like levels by the approximately octahedral crystal field. Two peaks are observed in this region separated by 2.3 eV, which agrees well with the crystal-field splitting of the Zr 4d band measured by XAS [9]. The second region shows a striking similarity with the initial structure at the silicon K edge and may be associated with transitions to states predominantly formed from silicon 3s/3p/3d orbitals hybridized with oxygen 2p orbitals, although the influence of zirconium 5s and 5p orbitals on the structure in the second region is not discounted. This interpretation of the oxygen K edge in zircon agrees well with studies of the oxygen K ELNES in rare-earth oxides [17].

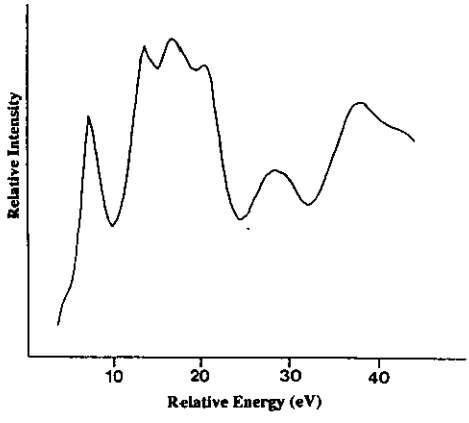

Figure 8. Plot showing the result of an MS calculation of the oxygen K edge in zircon for a cluster consisting of nine coordination shells.

Multiple-scattering calculations for a nine-shell cluster (figure 8) broadly support this interpretation. In the first region the calculation is unable to reproduce two peaks; however, the relative energy position of the one strong peak which is modelled is extremely sensitive to the particular zirconium phase shifts employed. Presumably the inability to reproduce the crystal-field splitting of the Zr 4d orbitals is related to the inaccurate description of the Zr scattering properties mentioned previously. In the second region the calculation fails to reproduce the fine structure observed in the experimental spectrum. However, the energy range over which peaks are present is similar in both calculation and experiment, and the shape is less sensitive to the zirconium phase shifts employed. This is taken as evidence that the oxygen K edge can be interpreted as two distinct regions, but the exact origin of the ELNES in the second region is uncertain.

6. Conclusions

In this paper all the major electron energy-loss edges for silicon, oxygen and zirconium in natural zircon have been reported. The silicon L_1 and K edge in zircon are noted to

exhibit identical ELNES, indicating that the effect of core-hole lifetime on comparing excitations from 1s and 2s core levels is small. The silicon K ELNES shows four peaks, different to that of α-quartz which exhibits only two peaks at the silicon K edge. In α-quartz these peaks arise from transitions to unoccupied MOs with t_2 symmetry. In zircon the symmetry of the SiO_4 polyhedron is reduced from T_d to D_{2d}, and this results in splitting of each t_2 level into two MOs, namely e and b_2. Thus, at the silicon K edge of zircon four peaks will occur, but MS calculations indicate that only the first pair of peaks can be identified as transitions to specific MOs. The intensity of the second pair of peaks is dependent on outer coordination shells.

The silicon $L_{2,3}$ edge of zircon is significantly different to that found in other simple silicates, and it has been shown that the complicated ELNES arises from distortion of the SiO_4 polyhedron. Using a combination of MO theory and the MS calculations an assignment of each peak in this spectrum to an unoccupied molecular orbital has been proposed. However, it should be noted that the precise MO assignments are dependent on the method of calculation employed. Nevertheless, the theoretical approaches clearly show that the unusual form of the silicon $L_{2,3}$ ELNES in zircon arises from the reduced symmetry, compared with α-quartz or fayalite, at the silicon site. As a result of this reduced symmetry the degeneracy of the unoccupied MOs is lifted, and hence, many extra peaks are observed at the silicon $L_{2,3}$ edge—precisely what is found experimentally.

The oxygen K-shell excitation shows very unusual near-edge structure and only limited success in modelling this edge using MS calculations has been achieved. It has not been possible to describe precisely the final states of the excited core electrons at this edge due to the lack of a suitable MO diagram on which an interpretation can be based. The oxygen K ELNES can be divided into two main regions. The first is associated with zirconium d-dominated empty states, while the second is ascribed to final states formed from silicon orbitals. The failure of the MS calculations to reproduce accurately the observed splitting in the first region, arising from the ZrO_8 crystal field, is due in part to the poor muffin-tin potential used to obtain the zirconium phase shifts.

The concept of a coordination fingerprint is one which is a useful starting point in the study of ELNES. However, in this paper it has been shown that great care must be taken in applying the concept too widely. The energy-loss spectra from zircon clearly illustrate this, since zircon, like α-quartz or fayalite, is a silicate mineral in which the primary structural unit is a silicon atom coordinated to four oxygen atoms. Often this SiO_4 unit exhibits approximately tetrahedral symmetry, but there are many cases where it does not, e.g. zircon. Energy-loss spectra from non-tetrahedral SiO_4 units will be significantly different to those of tetrahedral SiO_4 units, especially where the relative magnitude of the distortion is large. Therefore, the concept of coordination fingerprint is misleading. It is clearly more appropriate to classify ELNES in terms of a symmetry fingerprint.

In conclusion, only limited success in understanding the ELNES for zircon has been achieved using MO theory and MS calculations. For a more detailed interpretation using MS theory clearly an improvement on the muffin-tin potential used in the calculation must be obtained. A complete description of the observed ELNES using MO thoery will only be possible if MO calculations for each central atom, i.e. silicon, oxygen and zirconium, are carried out. However, it is clear that the observed ELNES is strongly affected by at least the second coordination shell, and therefore any MO calculation should be enlarged to include at least the second-nearest-neighbour atoms.

This will be costly in terms of computer time, and may still require refinement in order to interpret the ELNES. A more useful advance, although equally demanding computationally, would be to perform a full band-structure calculation for zircon, with the results presented as the symmetry-projected DOS at each atom site. However, until the results of such band-structure calculations are readily available, it is concluded that the combination of MO thoery with MS calculations provides an excellent starting point, from which a working description of the ELNES can be achieved.

Acknowledgments

We thank the Royal Commission for the 1851 Exhibition (DWM) and the Royal Society (RDB) for supporting this research, the Danish Council for Technical Research for funding during a one-year visit (PLH), and ICI plc for funding a two-year secondment (RSP) to the Cavendish Laboratory. We are grateful to Peter Rez, Yuan Jun, Phil Gaskell, Mick Brown, and Archie Howie for many stimulating discussions about this work. We also thank Bob Crick for his help in preparing figure 1.

References

[1] Egerton R F 1986 *Electron Energy Loss Spectroscopy in the Electron Microscope* (New York: Plenum)
[2] Brydson R 1991 *EMSA Bulletin (Fall Edition)*
[3] Robinson K, Gibbs G V and Ribbe P H 1971 *Am. Mineral.* **56** 782
[4] McComb D W, Brydson R and Hansen P L 1991 *Microsc., Microanal., Microstruct.* **2** 561
[5] Payne R S, Crick R A and McComb D W 1991 *Inst. Phys. Conf. Ser.* vol 119 (Bristol: Institute of Physics) p 113
[6] McMullan D, Rodenburg J M, Murooka Y and McGibbon A J 1989 *Inst. Phys. Conf. Ser.* vol 98 (Bristol: Institute of Physics) p 55
[7] Batson P E, Kavanagh K L, Wong C Y and Woodall J M 1987 *Ultramicroscopy* **22** 89
[8] Smyth J R and Bish D L 1988 *Crystal Structures and Cation Sites of the Rock-Forming Minerals* (Boston: Allen and Unwin)
[9] Thromat N, Noguera C, Gautier M, Jollet F and Duraud J P 1991 *Phys. Rev.* B **44** 7904
[10] Tossel J A 1975 *J. Am. Chem. Soc.* **97** 4840
[11] Frisch M J *et al* 1990 *GAUSSIAN 90 Revision I* (Pittsburgh, PA: Gaussian Incorporated)
[12] Rez P, Weng X and Ma H 1991 *Microsc., Microanal., Microstruct.* **2** 143
[13] Vvedensky D D, Saldin D K and Pendry J B 1986 *Comput. Phys. Commun.* **40** 421
[14] Cotton F A 1990 *Chemical Applications of Group Theory* (New York: Wiley)
[15] Hansen P L, Brydson R and McComb D W 1992 *Microsc., Microanal., Microstruct.* at press
[16] Wales D 1992 private communication
[17] Yuan J 1992 Direct evidence for the extended f states in CeO_2 in preparation
[18] Dehmer J L 1972 *J. Chem. Phys.* **56** 4496
[19] Friedrich H, Pittel B, Rabe P, Schwartz W H E and Sonntag B 1980 *J. Phys. B: At. Mol. Phys.* **13** 25
[20] Chelikowsky J R and Schluter M 1977 *Phys. Rev.* B **15** 4020
[21] Johansen H 1974 *Theor. Chim. Acta* **32** 273
[22] Pietro W J, Francl M M, Hehre W J, DeFrees D J, Pople J A and Binkley J S 1982 *J. Am. Chem. Soc.* **104** 5039